УДК 621.762

CRYSTALLOGRAPHIC STRUCTURE AND AC IMPEDANCE SPECTROSCOPY OF BININBVOX SOLID ELECTROLYTE

AHLAM AL-ALAS[1], MARWAN F. S. H. AL-KAMALI[2], NABIL S. SALAMI[3], NIYAZI A. S. AL-AREQI[1], ANDEI A. BOIKA[2]

[1]Department of Chemistry, Faculty of Applied Science, Taiz University, Republic of Yemen

[2]Educational institution "Sukhoi State Technical University of Gomel", the Republic of Belarus

[3]Department of Chemistry, Faculty of Education-Zabid, Hodeida University, Republic of Yemen

The research results of the crystallographic structure and spectroscopic AC impedance properties of a new twice substituted bismuthvanadatesynthesized as $Bi_2V_{1-x}(Ni_{1/3}Nb_{2/3})_xO_{5.5-\delta}$ (abbreviated BININBVOX) are presented. The synthesis was carried out by a simple solid-phase reaction at 750 °C for 20 h, for compositions $0.15 \leq x \leq 0.25$. The structure and phase composition were studied by X-ray diffraction analysis (XRD) and differential thermal analysis (DTA) during heat treatment. The results of AC impedance spectroscopy were used to evaluate the electrical properties of the BININBVOX system dependence on the temperature and dopant concentration. X-ray analysis (according to Rietveld) together with the DTA results showed clear stabilization of the tetragonal γ'-phase with the spatial group I4/m mm for all synthesized compositions at room temperature. The lattice dimensions slightly increased along the c axis and changed slightly along the a axis with an increase in the Ni–Nb(x) content. The calculated bond lengths of V–O(1) and V/Ni/Nb–O(3) were almost the same for all compositions, whereas V/Ni/Nb–O(2) and V/Ni/Nb–O(4) decrease significantly with increasing Ni-Nb content. This may be due to the increased substitution of V^{5+} for both Ni^{2+} and Nb^{5+} in the perovskite vanadate layers. The values of the measured dielectric permittivity at 300 and 600 °C showed a sharp rise with increase of the Ni–Nb dopant concentration, which indicates that the migration of oxygen vacancies and the accompanying charge accumulation in the perovskite-vanadate layers depend on the composition. It is interesting that the rise in the Ni–Nb dopant concentration significantly increased the overall BININBVOX electrical conductivity over the entire temperature range, which is also higher than that of the related single-substituted Ni/Nb in $Bi_2V_{O5.5}$.

Keywords: crystallography, BIMEVOX, AC spectroscopy, double substitution, doping.

КРИСТАЛЛОГРАФИЧЕСКАЯ СТРУКТУРА И СПЕКТРОСКОПИЯ ИМПЕДАНСА ПЕРЕМЕННОГО ТОКА ТВЕРДОГО ЭЛЕКТРОЛИТА BININBVOX

АХЛАМ АЛЬ-АЛАС[1], МАРВАН Ф. С. Х. АЛЬ-КАМАЛИ[2], НАБИЛ С. САЛАМИ[3], НИВАЗИ А. С. АЛЬ-АРИКИ[1], АНДРЕЙ А. БОЙКО[2]

[1]Кафедра химии, факультет естественных наук, Таизский университет, Республика Йемен

[2]Учреждение образования «Гомельский государственный технический университет имени П. О. Сухого», Республика Беларусь

[3]Кафедра химии, образовательный факультет, Ходейдинский университет, г. Забид, Республика Йемен

Представлены результаты исследования кристаллографической структуры и спектроскопических свойств импеданса переменного тока нового дважды замещенного ванадата висмута, синтезированного в виде $Bi_2V_{1-x}(Ni_{1/3}Nb_{2/3})_xO_{5.5-\delta}$ (сокращенно BININBVOX). Синтез проводили простой твердофазной реакцией

при 750 °С в течение 20 ч, для составов 0,15 ≤ x ≤ 0,25. Структуру и фазовый состав в процессе термообработки изучали с помощью рентгеноструктурного анализа (РФА) и дифференциального термического анализа (ДТА). Для оценки зависимости электрических свойств системы BININBVOX от температуры и концентрации легирующей примеси использовали результаты спектроскопии импеданса переменного тока. Анализ рентгенограмм (по Ритвельду) вместе с результатами ДТА ясно свидетельствовали о стабилизации тетрагональной γ′-фазы с пространственной группой I4/m mm для всех синтезированных составов при комнатной температуре. Размеры решетки незначительно увеличивались по оси c и незначительно менялись по оси a при увеличении содержания Ni–Nb(x). Расчетные длины связей V–O(1) и V/Ni/Nb–O(3) оказались практически одинаковыми для всех составов, тогда как V/Ni/Nb–O(2) и V/Ni/Nb–O(4) заметно уменьшается с увеличением содержания Ni–Nb. Это может быть связано с повышенным замещением V^{5+} как Ni^{2+}, так и Nb^{5+} в слоях перовскит-ванадата. Значения измеренной диэлектрической проницаемости при 300 и 600 °С показали резкое увеличение по мере увеличения концентрации легирующей примеси Ni–Nb, что указывает на то, что миграция кислородных вакансий и сопровождающее ее накопление заряда в слоях перовскит-ванадата зависят от состава. Интересно, что увеличение концентрации легирующей примеси Ni–Nb значительно увеличило общую электропроводность BININBVOX во всем диапазоне температур, которая также выше, чем у соответствующих однократно замещенных Ni/Nb в составе $Bi_2VO_{5.5}$.

Ключевые слова: кристаллография, BIMEVOX, спектроскопия переменного тока, двойное замещение, легирование.

Introduction

BIMEVOXes (BI = bismuth, ME = dopant metal ion, V = vanadium, and OX = oxide) constitute a family of layered Aurivillius-type compounds, derived by the partial substitution of Me for V in the parent compound-bismuth vanadate, $Bi_2VO_{5.5}$, and formulated as $Bi_2Me_xV_{1-x}O_{5.5-\delta}$. These functional materials were first discovered by Abraham, F. et al. in 1990 [1], and then extensively investigated by several researchers for their structure, phase changes and ionic conductivity upon a metal doping [2], [3].

The BIMEVOXes like the parent compound are structurally shown as intergrowth of two alternating bismuthate layers; a bismuthate layer, Bi_2O_2 with square pyramidal coordination and a perovskite vanadate layer, $V_{1-x}Me_xO_{3.5}\delta_{0.5}$, where δ stands for an oxide ion vacancy [4]–[6]. The ionic conductivity in $Bi_2VO_{5.5}$ and their derivates, BIMEVOXes is entirely attributed to the existence of such vacancies in the perovskite vanadate layers which thereby facilitate the mobility of oxide ion through. The vacancy ordering in the perovskite vanadate layer $Bi_2VO_{5.5}$ is associated with the occurrence of two-phase transitions; monoclinic-α to orthorhombic-β at 447 °C, and β to tetragonal-γ at 567 °C [7].

Many attempts have been made for enhancement of their ionic conductivity by either a single substitution [8]–[13] or double substitution [14]–[16] of transition metal ions which led to the stabilization of highly conducting tetragonal, γ′-phase at room temperature and conferred the stabilized γ-phase a promising application as a polycrystalline solid electrolyte for intermediate temperature-solid oxide fuel cells (IT-SOFCs). Among these, γ-BINIVOX showed better ionic conduction and high performance, as its ionic conductivity reached ~ 0.1 S cm^{-1} at 600 °C [17].

The ionic conductivity of substituted bismuth vanadate in the range of 0.1 at 600 °C and lead to better ionic conduction and high performance of this family at low temperature.

The main aim of this paper is to present a detailed investigation on crystallographic structure and AC impedance spectroscopic properties of a new BIMEVOX obtained by the partial substitution of 1/3 Ni^{2+} and 2/3 Nb^{5+} for V^{5+} site of the parent compound, using a conventional solid-state reaction at 750 °C. The resulting compound is formulated as $Bi_2V_{1-x}(Ni_{1/3}Nb_{2/3})_xO_{5.5-\delta}$, and acronymized as BININBVOX. This study has been carefully performed by focusing on three compositions (i. e., x = 0.15, 0.20, and 0.25), where the conducting tetragonal, γ′-phase is effectively stabilized at room temperature.

Materials & Methods

Sample synthesis

Accurate molar amounts of starting materials, as per the following balanced equation, were thoroughly mixed, and grinded together with analytical-grade acetone using agate mortar for homogeneity:

$$Bi_2O_3 + \frac{(1-x)}{2}V_2O_5 + \frac{x}{3}NiO + \frac{x}{3}Nb_2O_5 \rightarrow Bi_2V_{1-x}(Ni_{1/3}Nb_{2/3})_xO_{5.5-\delta}.$$

The resulting paste was then calcined in air at 750 °C for 20 h with intermediate cooling and grinding with acetone to obtain pure microcrystalline powder. The final calcined powder was isostatically pressed into pellets with same dimensions; 13 mm diameter and 1 mm thickness using Spectra-lab SL-89 at 350 MPa.

Crystallography

Powdered samples of the BININBVOX system were investigated by XRD using *a Rigaku/Max-B X-ray diffractometer* with Ni-filtered CuK_α radiation (λ = 1.54060 Å). Data were recorded with the Bragg–Brentano geometry at a scan time of 0.6 s/increment in the range $5° \le 2\theta \le 90°$. The unit cell and bond parameters were calculated by the *Rietveld* refinement method using the *X' Pert Plus* software program.

Differential thermal analysis

The DTA measurements were performed using *a Shimazu SC-TA 60 Thermal Analyzer*. About 20 mg of BININBVOX sample were heated in in a nitrogen atmosphere supplied at a flow rate of 100 mL min^{-1} from 40 to 900 °C at a constant heating rate of 10 °C min^{-1}.

Electrical measurements

The prepared pellets were sintered at 750 °C in a muffle furnace for 5 h. The silver paste was applied for coating both pellet faces. AC impedance measurements were carried out in air in the frequency range 20 Hz–1 MHz using *a Wayne Kerr LCR Meter 41.00* from 100 to 700 °C in a step of 20 °C with 20 min stabilization time for each measurement. The values of circuit parameters were estimated by non-linear least square fitting using *Zview* software program. The complex impedance can be written as complex number $Z(\omega) = Z' + Z''$, where Z' represents the real part of impedance and Z'' represents the imaginary part of impedance. The total resistance below ~ 400 °C is equal resistance of grain and grain boundary, $R_t = R_g + R_{gb}$. The total conductivity is calculated as $\sigma = L/(R_tA)$, where L/A is the thickness/area ratio of pellet. At higher temperature the resistance is obtained from the intercept of line inclined with real axis Z' ($R_t = Z'_{\text{intercept}}$). The total conductivity was depicted as Arrhenius plot ($\log\sigma T$ *vs.* $1/T$). The dielectric permittivity had been determined at constant frequency 1Hz. The dielectric constant calculated using the equation $\varepsilon = (C_{1\text{MHz}}/\varepsilon°) \times (L/A)$, where $\varepsilon°$ is the permittivity of free space (8.854×10^{-14} F cm^{-1}).

Results & Discussion

Figure 1 shows the XRD patterns of the $Bi_2V_{1-x}(Ni_{1/3}Nb_{2/3})_xO_{5.5-\delta}$ system measured at room temperature and refined by the Rietveld method using $Bi_2V_{0.8}Co_{0.2}O_{5.2}$ as the starting model [2]. Agreed with DTA results (not presented here), the Rietveld refinement clearly evidences the stabilization of tetragonal, γ'-phase with a space group, I4/m mm for all synthesized compositions at room temperature. The values of refined unit cell parameters, crystallite size (D), and crystallographic density (d_{XRD}) are summarized in Table 1. It can be observed that the lattice dimensions slightly increase along *c*-axis and insignificantly change along *a*-axis as the Ni–Nb content (x) increases. However, the a and c parameters refined for all compositions of the $Bi_2V_{1-x}(Ni_{1/3}Nb_{2/3})_xO_{5.5-\delta}$ system are remarkably greater

than those for the first composition with stabilized γ'-phase in the single Ni-substituted $Bi_2VO_{5.5-\delta}$ system, i. e. $Bi_2V_{0.87}Ni_{0.13}O_{5.405-\delta}$, as reported earlier [3].

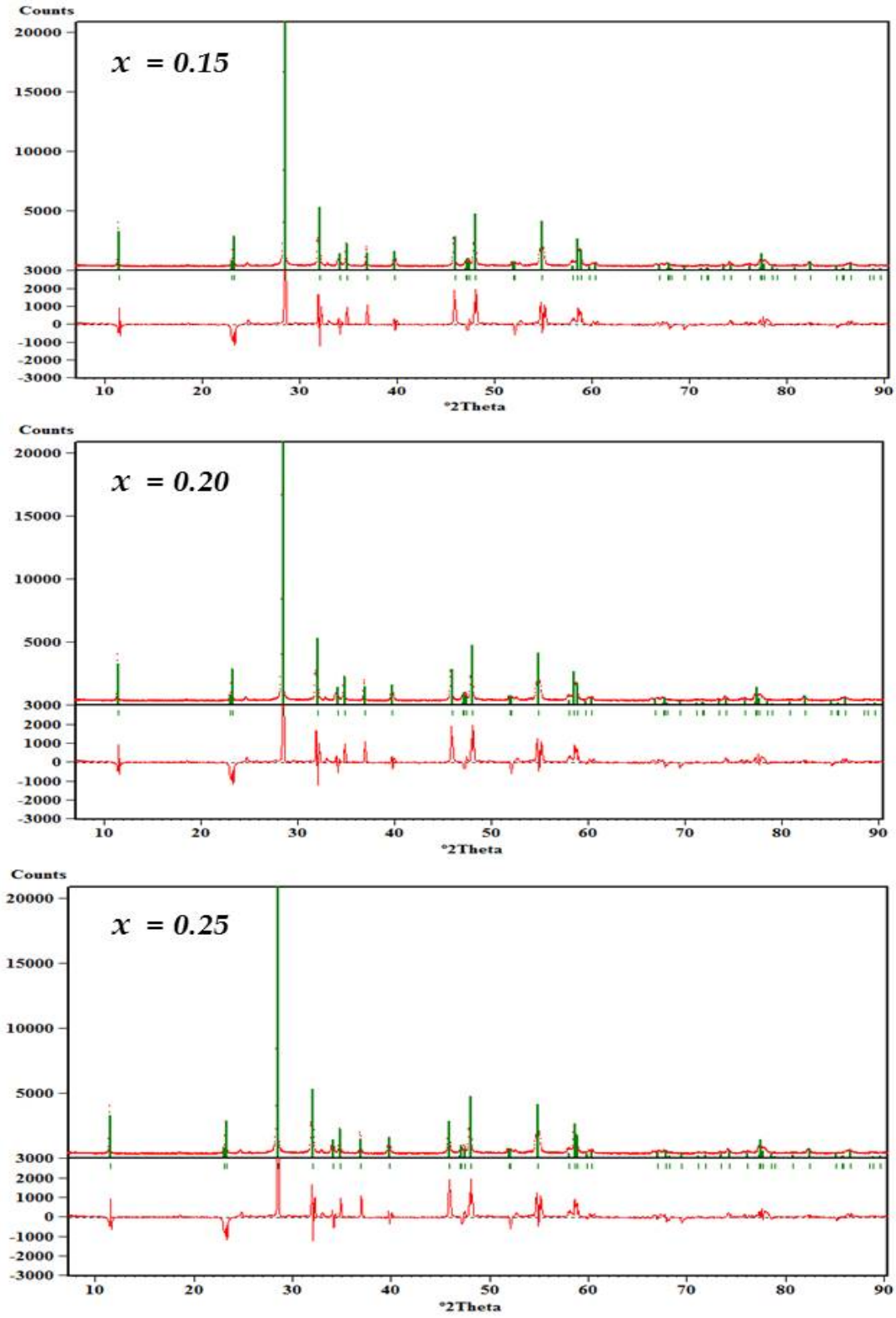

Fig. 1. Rietveld-refined XRD patterns of the $Bi_2V_{1-x}(Ni_{1/3}Nb_{2/3})_xO_{5.5-\delta}$ system for various compositions measured at room temperature

Table 1

Refined unit cell parameters, phase stabilization, average crystallite sizes and crystallographic densities of as-prepared samples of the $Bi_2V_{1-x}(Ni_{1/3}Nb_{2/3})_xO_{5.5-\delta}$ system

x	Unit cell parameters			Phase stabilization		D(μm)	d_{XRD} (g cm^{-3})	R_p%	R_{wp}%	R_{exp}%
	a (Å)	c (Å)	V(Å^3)	Phase	Space group					
0.15	3.975(5)	15.388(5)	122.35(4)	γ'	I4/m mm	4.96	6.47	5.83	8.19	5.87
0.20	3.973(2)	15.392(3)	122.31(3)	γ'	I4/m mm	4.87	6.52	5.56	7.64	5.33
0.25	3.977(4)	15.398(7)	122.49(4)	γ'	I4/m mm	4.92	6.53	6.34	6.82	6.27

The idealized Aurivillius-type structure of $Bi_2V_{1-x}(Ni_{1/3}Nb_{2/3})_xO_{5.5-\delta}$ is illustrated in Fig. 2, which is built of alternating pyramidal bismuthate, $(Bi_2O_2)^{2+}$ layers and perovskite substituted vanadate, $(V/Ni/NbO_{3.5}\delta_{0.5})^{2-}$ layers, where δ stands for an oxygen vacancy. In the perovskite vanadate layer, two apical oxygen sites; O(1) and O(3), and two equatorial oxygen sites; O(2) and O(4) were involved in the refinement as partially occupied, while the occupancy of V/Ni/Nb remained constant as per the calculated stoichiometry of the prepared compositions. An equivalent oxygen site, O(5) of the bismuthate layer was considered as fully occupied. It is interesting to appoint that the occupancy numbers of O(1) and O(3) remain almost same for all compositions, while that of O(2) and O(4) decrease with increasing Ni–Nb content, indicating an increased oxygen vacancy concentration in the equatorial planes of perovskite vanadate layers [4]–[6].

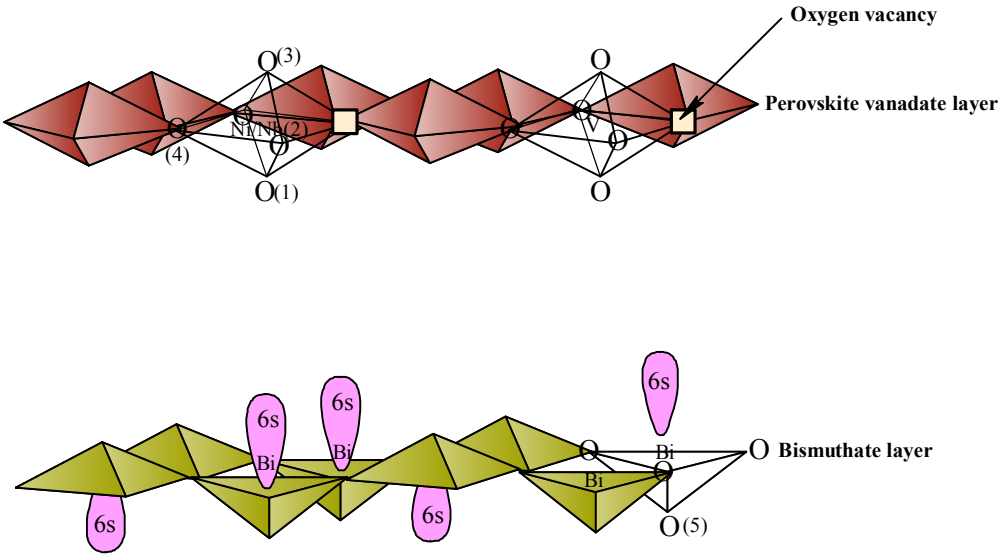

Fig. 2. Layered Aurivillius-type structure of $Bi_2V_{1-x}(Ni_{1/3}Nb_{2/3})_xO_{5.5-\delta}$

Some selected bond lengths of perovskite vanadate and bismuthate layers for the $Bi_2V_{1-x}(Ni_{1/3}Nb_{2/3})_xO_{5.5-\delta}$ system are listed in Table 2. It is clearly observed that the bond lengths of V–O(1) and V/Ni/Nb–O(3) remain almost same for all compositions, while that of V/Ni/Nb–O(2) and V/Ni/Nb–O(4) remarkably decrease as the Ni–Nb content increases. This can be attributed to the increased substitution of both Ni^{2+} and Nb^{5+} for V^{5+} in the vanadate layers. Moreover, the constancy in the bond lengths of Bi–Bi, Bi–O(5), and

O(5)−O(5) with all compositions is also evidence for the substitution of only V in the vanadate layers by Ni and Nb, as revealed by the XRD Rietveld refinement.

Table 2

Variation of some important bond lengths of the $Bi_2V_{1-x}(Ni_{1/3}Nb_{2/3})_xO_{5.5-\delta}$ system with composition

Layer	Bond	Bond length (Å)		
		$x = 0,15$	$x = 0,20$	$x = 0,25$
Vanadate	V−O(1)	1.543(3)	1.545(6)	1.546(2)
	V/Ni/Nb−O(2)	1.598(7)	1.593(4)	1.592(4)
	V/Ni/Nb−O(3)	1.746(2)	1.747(4)	1.745(2)
	V/Ni/Nb−O(4)	1.896(8)	1.892(7)	1.890(3)
	O(1)−O(2)	2.646(9)	2.652(1)	2.656(4)
	O(2)−O(3)	2.355(4)	2.356(4)	2.359(1)
	O(3)−O(4)	2.466(1)	2.471(3)	2.468(2)
	O(1)−O(4)	2.716(3)	2.718(4)	2.719(3)
Bismuthate	Bi−Bi	2.918(6)	2.917(5)	2.917(4)
		2.754(2)	2.754(6)	2.754(4)
	Bi−O(5)	2.341(2)	2.342(3)	2.341(6)
	O(5)−O(5)	2.716(3)	2.716(7)	2.716(7)

Complex plane plots of AC impedance data scanned at 260 °C for equally dimensional sintered pellets of all compositions are shown in Fig. 3. For each composition, two depressed semicircular arcs are clearly observed in all presented plots. A large high-frequency arc is assigned to the grain interior contribution, and the low-frequency arc represents the minor contribution of grain boundaries. However, beyond the letter the scanned impedance data takes the form of a curved inclined spike at the extreme low-frequency terminal which reflects the impedance contribution of the electrode-electrolyte interface. The interesting point to be emphasized here is that the two semicircular arcs drastically disappear with increasing temperature upto ~ 440 °C, where the impedance data behind this temperature can be visualized as the only inclined spike (not presented here) as a consequence of the limited instrumental frequency range and the rapid increase of impedance – time response as a function of temperature [7]. The typical electric equivalent circuit applied for fitting of the impedance data is presented as an inset of Fig. 3, which models the three aforementioned contributions below ~ 360 °C for all compositions. A non-linear least squares method was applied to fit the impedance data using *Zview* software program, where χ^2 and *WSS* were taken into account for testing the validity of fitting procedure. The estimate values of the equivalent circuit parameters obtained from the impedance plots shown in Fig. 3 are illustrated in Table 3. It can be observed that the values of R_g are much greater than that of R_{gb}, and CPE_{gb} is found to be 100 times greater than CPE_g for all compositions. This indicates that the contribution of the grain interiors to the total ionic conductivity is much more pronounced compared to that of grain boundaries, and that the permittivity associated with charge accumulation predominantly increases at the vicinity of grain boundaries. However, the noticeable decrease of τ_g with increasing Ni–Nb content suggests the short-range diffusion of oxygen vacancies within the grains as observed for singly substituted systems [8], [9], as well as doubly substituted one [18].

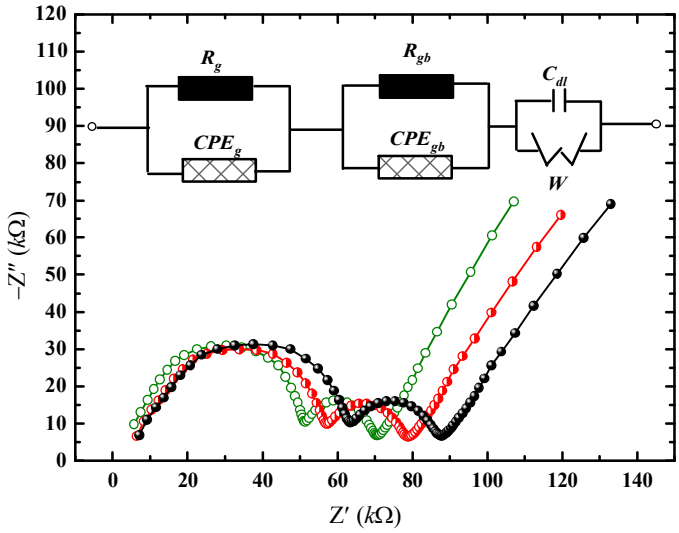

Fig. 3. Complex impedance plane plots of the $Bi_2V_{1-x}(Ni_{1/3}Nb_{2/3})_xO_{5.5-\delta}$ system for various compositions measured at 260 °C. The inset shows the equivalent circuit model used for fitting the impedance data: R_g – resistive contribution of grain interiors; R_{gb} – resistive contribution of grain boundaries; CPE_{gb} – constant phase element of grain interiors; CPE_{gb} – constant phase element of grain boundaries; W – Warburg impedance element; Cdl – double layer capacitance: – $x = 0.15$; – $x = 0.22$; – $x = 0.25$

Table 3

Refined equivalent circuit parameters deduced from impedance plane plots measured at 260 °C for the $Bi_2V_{1-x}(Ni_{1/3}Nb_{2/3})_xO_{5.5-\delta}$ system

Equivalent circuit parameters	$Bi_2V_{1-x}(Ni_{1/3}Nb_{2/3})_xO_{5.5-\delta}$ compositions		
	$x = 0.15$	$x = 0.20$	$x = 0.25$
$R_g(\times10^3)$, Ω	64.38	58.26	53.43
$R_{gb}(\times10^3)$, Ω	21.76	20.02	18.25
$C_g(\times10^{-10})$, F	3.46	3.21	2.88
$C_{gb}(\times10^{-8})$, F	6.56	6.37	6.06
$W(\times10^{-4})$, F	4.33	4.87	5.62
$C_{dl}(\times10^{-3})$, F	2.74	3.58	3.89
$\tau_g(\times10^{-5})$, s	2.23	1.87	1.54
$\tau_{gb}(\times10^{-3})$, s	1.43	1.28	1.11
$\chi^2(\times10^{-3})$	1.18	1.02	1.16
WSS	0.155	0.121	0.142

*χ^2 and *WSS* represent the validation parameters of non-linear fitting procedure.

The dielectric permittivity, ε was computed from CPE_{2MHz}, the value of the constant phase element at a frequency of 2 MH*z* corresponding to the real part of complex plane plot. Figure 4 presents logε-*T plots* of the $Bi_2V_{1-x}(Ni_{1/3}Nb_{2/3})_xO_{5.5-\delta}$ system on the first heating run. The temperature corresponding to the subtle discontinuity observed for each plot can be considered as the $\gamma' \rightarrow \gamma$ transition temperature, which could not be detected in the DTA thermograms of the $Bi_2V_{1-x}(Ni_{1/3}Nb_{2/3})_xO_{5.5-\delta}$ system. The values of ε at 300 and 600 °C are listed in Table 4, which show a drastic increase as Ni–Nb dopant concen-

tration increases, indicating that the oxygen-vacancy migration and accompanied charge accumulation in the perovskite vanadate layers are compositionally dependent.

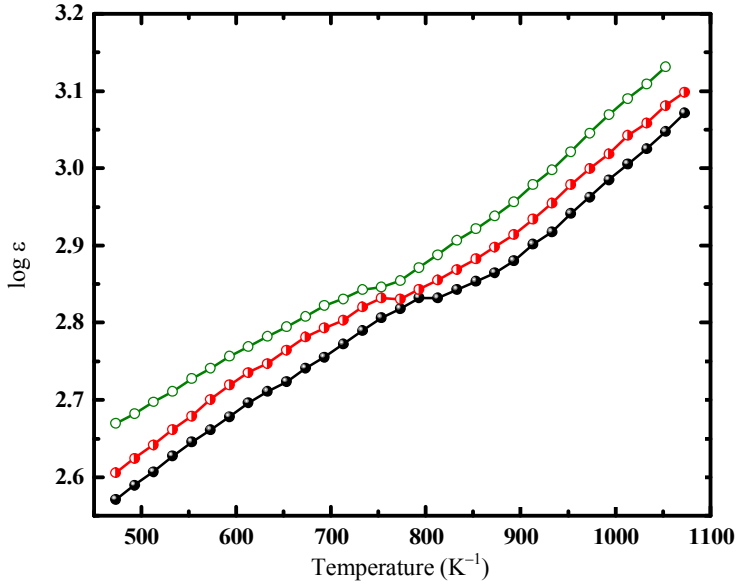

Fig. 4. Temperature dependence of dielectric permittivity on heating run for the $Bi_2V_{1-x}(Ni_{1/3}Nb_{2/3})_xO_{5.5-\delta}$ system:
– $x = 0.15$; – $x = 0.20$; – $x = 0.25$

Table 4

Estimate values of the dielectric permittivity, electrical conductivity, and activation energy of conduction of the $Bi_2V_{1-x}(Ni_{1/3}Nb_{2/3})_xO_{5.5-\delta}$ system at high- and low-temperature region

x	ε_{300}	σ_{300} (S cm^{-1}) × 10^{-4}	ε_{600}	σ_{600} (S cm^{-1}) × 10^{-2}	$E_{a(1)}$ (eV)	R^2	$E_{a(2)}$ (eV)	R^2
0.15	458.14	0.77	731.13	2.29	0.53	0.9937	0.89	0.9945
0.20	502.34	1.48	790.68	4.48	0.54	0.9965	0.86	0.9941
0.25	553.35	2.31	868.96	5.67	0.57	0.9968	0.77	0.9980

The total electrical conductivity, σ was deduced from impedance data considering the total resistance, $R_t = R_g + R_{gb}$ at temperatures below ~ 440 °C, and the value of Z' to which the inclined spike is extrapolated at temperatures higher than ~ 440 °C, where the two semicircular arcs can not be recognized well in the impedance plane plots. Arrhenius plots of electrical conductivity of the $Bi_2V_{1-x}(Ni_{1/3}Nb_{2/3})_xO_{5.5-\delta}$ system on heating run are shown in Fig. 5. Two lines of different slopes are visualized in each plot due to the $\gamma' \rightarrow \gamma$ transition with a discontinuity temperature approximately similar to that observed in the corresponding temperature dependence of dielectric permittivity (Fig. 4). Values of activation energies of electrical conduction, $E_{a(1)}$, and $E_{a(2)}$ computed from two different slopes in the temperature regions, 200–380 °C, and 440–800 °C, respectively for all compositions are seen in Table 4 along with the measured values of σ at 300 and 600 °C. Interestingly, the increase of Ni–Nb dopant concentration remarkably enhances the total conductivity over whole temperature range, except some anomalies in the region of discontinuities. This is accompanied with a slight increase of $E_{a(1)}$, and lowering in $E_{a(2)}$. The interesting point to be emphasized here is that the total electrical conductivities of the $Bi_2V_{1-x}(Ni_{1/3}Nb_{2/3})_xO_{5.5-\delta}$ sys-

tem are higher than those of corresponding singly Ni/Nb substituted $Bi_2VO_{5.5}$. This evidences that the Ni–Nb double substitution enhances the ionic conductivity of the BIMEVOX material due to the optimal matching of Ni^{2+} and Nb^{5+} radii in the perovskite vanadate layer, resulting in reduction of association energy between oxide-ion vacancy and both Ni and Nb ions. Similar results have also been reported for the Ti–Nb substituted bismuth vanadate [19].

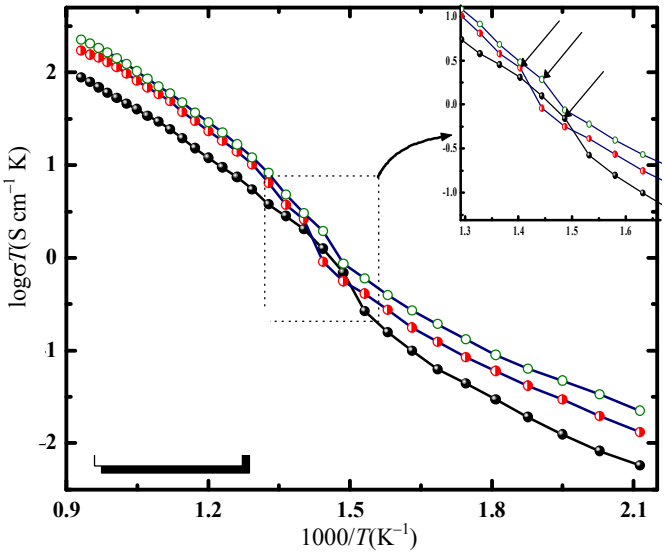

Fig. 5. Arrhenius plots of total electrical conductivity on heating run for the $Bi_2V_{1-x}(Ni_{1/3}Nb_{2/3})_xO_{5.5-\delta}$ system: – $x = 0.15$; – $x = 0.20$; – $x = 0.25$

Conclusions

The crystallographic structure and electrical properties of a new BININBVOX system were carefully investigated for the following compositions: $x = 0.15$, 0.20, and 0.25, where the conducting tetragonal, γ′-phase is effectively stabilized at room temperature. Interestingly, the occupancy numbers of O(1) and O(3) remained almost same for all compositions, while that of O(2) and O(4) decreased with increasing Ni–Nb content, indicating an increased oxygen vacancy concentration in the equatorial planes of perovskite vanadate layers. This has been reflected by enhancement of electrical properties of the BININBVOX system as compared with singly substituted Ni/Nb systems, due to the optimal matching of Ni^{2+} and Nb^{5+} radii in the perovskite vanadate layer, resulting in reduction of association energy between oxide-ion vacancy and both Ni and Nb ions.

References

1. The bimevox series: a new family of high performances oxide ion conductors / F. Abraham [et al.] // Solid State Ionics. – 1990. – Vol. 40/41. – P. 934–937.
2. Abraham, I. Defect structure of quenched γ-BICOVOX by combined X-ray and neutron powder diffraction / I. Abraham, F. Krok, J. A. G. Nelstrop // Solid State Ionics. – 1996. – Vol. 90. – P. 57–65.
3. Photodegradation of 4-SPPN dye catalyzed by Ni(II)-substituted $Bi_2VO_{5.5}$ system under visible light irradiation: Influence of phase stability and perovskite vanadate-oxygen vacancies of photocatalyst / N. A. S. Al-Areqi [et al.] // Journal of Molecular Catalysis A: Chemical. – 2014. – Vol. 381. – P. 1–8.

4. Abrahams, I. Defect chemistry of the BIMEVOXes / I. Abrahams, F. Krok // J. Mater. Chem. – 2002. – Vol. 12. – P. 3351–3362.
5. Some features of the preparation, structure, and properties of BICUTIVOX / E. S. Buyanova [et al.] // Russ. J. Inorg. Chem. – 2011. – Vol. 56. – P. 1853–1857.
6. Tripathy, D. Studies on structural and optical properties and its correlation with the ionic conductivity of the $Bi_2VO_{5.5\text{-based}}$ oxide ionic conductors / D. Tripathy, A. Pandey // Solid State Ionics. – 2019. – Vol. 341. – P. 115038.
7. Beg, S. Layered Aurivillius compound: Synthesis, characterization and electrical properties / S. Beg, A. Al-Alas, N. A. S. Al-Areqi // Journal of Alloys and Compounds. – 2010. – Vol. 504. – P. 413–419.
8. Hervoches, C. H. Synthesis by the polymeric precursor technique of $Bi_2Co_{0.1}V_{0.9}O_{5.35}$ and electrical properties dependence on the crystallite size / C. H. Hervoches, M. C. Steil, R. Muccillo // Solid State Sci. – 2004. – Vol. 6. – P. 173–177.
9. Effect of niobium doping on structural, thermal, sintering and electrical properties of $Bi_4V_{1.8}Cu_{0.2}O_{10.7}$ / M. Alga [et al.] // Journal of Solid State Chemistry. – 2005. – Vol. 178. – P. 2873–2879.
10. Phase classification, electrical conductivity, and thermal stability of $Bi_2(V_{0.95}TM_{0.05})O_{5.5+\delta}$ (TM: transition metal) / Y.-k. Taninouchi [et al.] // Solid State Ionics. – 2010. – Vol. 181. – P. 1279–1286.
11. Gebicki, Relaxation dispersion of ionic conductivity of BICOVOX / A. Kezionis [et al.] // Solid State Ionics. – 1999. – Vol. 119. – P. 145–150.
12. Influence of dopant concentration on the phase transition and ionic conductivity in BIHFVOX system / S. Beg [et al.] // Physica B. – 2009. – Vol. 404. – P. 2072–2079.
13. Local structure in a tetravalent-substituent BIMEVOX system: BIGEVOX / Y. Yue [et al.] // J. Mater. Chem. A. – 2022. – Vol. 10. – P. 3793–3807.
14. Beg, S. Study on the electrical properties of Co–Ti double substituted $Bi_4V_2O_{11}$ / S. Beg, N. S. Salami // J. Alloys and Compounds. – 2014. – Vol. 586. – P. 302–307.
15. Beg, S Effect of Zn–Ti double substitution on the electrical properties of $Bi_4V_2O_{11}$ / S. Beg, N. S. Salami // Phase Transitions. – 2015. – Vol. 89. – P. 167–179.
16. Paydar, M. H. Studies on preparation, characterization and ion conductivity of TI–CU double substituted $Bi_4V_2O_{11}$ / M. H. Paydar, A. M. Hadian, G. Fafilek // Journal of the European Ceramic Society. – 2001. – Vol. 21. – P. 1821–1824.
17. Structural and electrical characterisation of BINIVOX / F. Krok [et al.] // Solid State Ionics. – 1998. – Vol. 111. – P. 37–43.
18. Role of Al and Ti doping in modulating electrical properties of BIVOX system / D. Tripathy [et al.] // Journal of Advanced Ceramics. – 2019. – Vol. 8. – P. 489–499.
19. Tripathy, D. Effect of simultaneous Ti and Nb doping on structure and ionic conductivity of $Bi_2V_{1-x}Ti_{x/2}Nb_{x/2}O_{5.5-\delta}$ ($0.1 \leq x \leq 0.25$) ceramics / D. Tripathy, A. Saikia, A. C. Pandey // Ionics. – 2019. – Vol. 25. – P. 2221–2230.

Получено 18.08.2022